





## Smoke Control Characteristics in Tunnel Fires under the Combined Effect of Air Curtains and Shafts



Peng Li , Xinru Tong\* , Xiaohua Jin , Yang Xu , Mengnan Kou

School of Energy & Environment, Zhongyuan University of Technology, Zhengzhou 450007, China

Corresponding Author Email: [2022108372@zut.edu.cn](mailto:2022108372@zut.edu.cn)

Copyright: ©2024 The authors. This article is published by IETA and is licensed under the CC BY 4.0 license (<http://creativecommons.org/licenses/by/4.0/>).

<https://doi.org/10.18280/ijht.420519>

### ABSTRACT

**Received:** 6 May 2024

**Revised:** 20 August 2024

**Accepted:** 12 September 2024

**Available online:** 31 October 2024

#### Keywords:

*tunnel fire, smoke control air curtain, shaft, smoke extraction efficiency, FDS numerical simulation*

Based on the characteristics of tunnel fires, numerical simulations using the Fire Dynamics Simulator (FDS) were conducted to explore the distribution characteristics of temperature, visibility, and carbon monoxide (CO) concentration, as well as smoke control effectiveness, by combining natural smoke extraction through shafts with smoke control via air curtains. The influence of air curtain jet velocity and angle and the distance between the air curtain and the shaft on these parameters was investigated. Results indicate that the natural smoke extraction of shafts and smoke control via air curtains work synergistically. However, the smoke control efficiency of the air curtain decreases as the distance between the air curtain and the shaft decreases, while the smoke extraction efficiency of the shaft follows an opposite trend. The smoke control efficiency of the air curtain was found to improve by 96.5% compared to conditions without a shaft. When the fire power was set at 12 kW, optimal angles for smoke control and extraction were identified as 30°, 20°, and 0° for air curtain jet velocities of 6 m/s, 8 m/s, and 10 m/s, respectively. In comparison to conditions without an air curtain, the shaft extraction efficiency increased by 140%. The temperature under the tunnel ceiling within the shaft distance increased with the air curtain jet velocity, while the temperature distribution in the areas outside the shaft distance exhibited the opposite trend. At eye level within the tunnel space, temperature and CO concentration increased with the air curtain jet velocity. Visibility in the smoke control area improved with increasing air curtain jet velocity, while visibility in the evacuation area showed an opposite trend. The temperature in the tunnel evacuation area stabilized below 60°C, with visibility remaining above 10 m and CO concentration below 50 ppm, thereby meeting the escape requirements for personnel. These findings further validate the feasibility of the combined air curtain and shaft smoke extraction model, providing a foundation for the design of smoke control systems in complex tunnel fire scenarios.

## 1. INTRODUCTION

With the development of the transportation industry, tunnels have become an essential component of modern transportation systems due to their convenience and minimal impact on surface traffic and river navigation. In recent years, the total number, length, and overall construction scale of tunnels have been increasing annually. As of 2022, there were 24,850 highway tunnels in China, with a total length reaching 26,784.3 extension meters. On the other hand, while tunnel transportation offers convenience to commuters, the high density of tunnels has led to an increase in tunnel fire incidents, resulting in significant property losses for both individuals and the government. Therefore, tunnel safety has become a crucial consideration during tunnel construction. Tunnels are generally enclosed and elongated. In the event of a fire, hot air mixed with dense smoke can rapidly spread to evacuation areas [1, 2]. Data indicate that smoke asphyxiation and toxic gases during tunnel fires account for approximately 85% of casualties [3].

Natural smoke extraction methods employed during tunnel

fires are generally classified into natural longitudinal ventilation and shaft ventilation. In recent years, shaft ventilation has gained widespread application in shallow-buried road tunnels, demonstrating effective ventilation results [4]. Wang et al. [5] highlighted the significant impact of shafts on smoke dispersion during tunnel fires, noting that the number of shaft openings is directly proportional to the intensity of the chimney effect, with higher temperatures observed at the junction of the main tunnel and the shaft. Building upon traditional shaft designs, Zhu et al. [6] introduced a novel mechanical plate-coupled ventilation shaft through scaled experiments, demonstrating that the new ventilation shaft effectively improves smoke extraction efficiency and thermal capacity while significantly reducing the occurrence of blockage phenomena. Additionally, Zhang et al. [7] found that wider tunnels and larger shaft opening areas contribute to the occurrence of the shaft suction phenomenon. They derived a new predictive model that considers the distance between the fire source and the shaft to estimate the critical shaft height for natural smoke extraction in tunnels.

In addition, some scholars have also investigated the impact of shaft shape on ventilation and smoke extraction performance. Results indicate that the total mass flow rate within a shaft increases with both the length and height of the shaft, with a greater sensitivity observed towards shaft length [8]. Additionally, studies using reduced-scale tunnel fire experiments have explored the natural ventilation performance of multi-shaft tunnel fires, establishing a simple model to predict smoke dispersion and temperature distribution under the tunnel ceiling. This research has examined the influence of shaft height and the heat release rate of the fire source on smoke patterns and extraction efficiency under the tunnel ceiling [9, 10]. As a flexible smoke control structure, the effectiveness of air curtains or mist curtains in mitigating hot smoke hazards during tunnel fires is crucial [11, 12]. Some scholars have proposed using air curtains to partition areas with differing environmental characteristics, thus preventing the transfer of smoke, heat, mass, and momentum between these areas. Air curtains can also create isolation zones to limit the heat and toxic gases released during tunnel fires [13, 14]. Existing research on air curtains primarily focuses on different structural configurations, such as single/double jet air curtains, counterflow air curtains, and blow-suction air curtains, analyzing their application characteristics in various fire scenarios [15-17]. Furthermore, studies have investigated how the dimensions of air curtains affect their smoke control effectiveness [18-20].

Based on the research on shafts and air curtains mentioned above, it can be observed that current studies on natural smoke extraction through shafts mainly focus on the effects of fire source location, power, and shaft dimensions on the tunnel disaster process and smoke extraction efficiency. There is comparatively limited research on the shafts themselves and their synergistic effects with other smoke control and extraction measures. Similarly, investigations concerning air curtains predominantly emphasize the optimization of various structural and dimensional parameters, while there is insufficient exploration of the combined effects of air curtains and the more cost-effective shaft smoke extraction measures. Therefore, this study introduces an air curtain smoke control system based on natural smoke extraction through shafts, aiming to explore the influence of air curtains on smoke spread and temperature distribution under varying fire source powers, as well as their smoke-blocking performance. The impact of working conditions of air curtains on the smoke extraction efficiency of shafts was also analyzed, providing reference

data for the future application of air curtains and shafts in various tunnel scenarios. This study is expected to contribute practical value to the promotion and utilization of air curtains and shafts.

## 2. NUMERICAL SIMULATION AND PARAMETER COMPUTATION

### 2.1 Modelling

An air curtain tunnel model was established using the FDS. The structural layout and positioning of measurement points are illustrated in Figure 1. The tunnel dimensions were set at 160 m in length, 10 m in width, and 5 m in height. Concrete with a thermal conductivity of 1.04 kJ/(kg·K) was used as the inner lining material. The initial fire environment conditions were configured with an ambient temperature of 20°C and an ambient pressure of 0.1013 MPa, while the initial smoke concentration was set to zero. To closely replicate realistic turbulent planar jet conditions, the synthetic eddy method (SEM) was employed to simulate the jet inlet boundary of the air curtain, with a turbulence intensity of 10% utilized for the vortex simulation. Both ends of the tunnel were configured in "OPEN" mode to connect with the external environment, while the tunnel wall was insulated from thermal exchange with the outside.

According to the National Fire Protection Association (NFPA) 502-2017 standard, the heat release rate of a burning truck is specified to range between 10 kW and 15 kW [21]. The truck fire was simplified into a fire source model with dimensions of 4 m × 2 m × 1.5 m, positioned at the central axis of the tunnel. The smoke control air curtain was installed on the tunnel ceiling, with the air curtain discharge length matching the tunnel width. The air curtains were placed at both ends of the shafts, with a distance of 60 m between the two shafts, and each shaft measuring 2 m × 2 m × 5 m. The air curtains were symmetrically positioned on either side of the fire source. The "SUPPLY" attribute within the FDS "SURFACE" module was utilized to modify the jet angle of the air curtain by adjusting its tangential velocity. The fuel source was specified as n-heptane, and a non-steady t<sup>2</sup> ultra-rapid fire model was employed, with a fire growth coefficient set at 0.188. A simulation duration of 360 s was selected for the analysis.

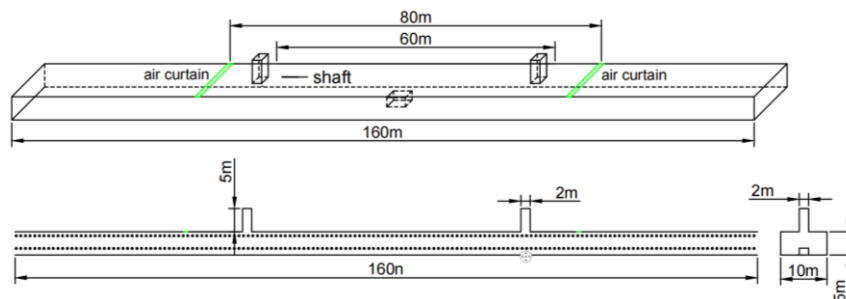


Figure 1. Schematic diagram of the tunnel model and measurement points

### 2.2 Smoke control efficiency

The effectiveness of smoke control is fundamentally achieved through the use of air curtains to separate regions with differing environmental characteristics, thereby

preventing the transfer of smoke, heat, mass, and momentum between these areas. Consequently, the smoke control efficiency of the air curtain can be represented by the degree of attenuation of thermal flux both in front of and behind the air curtain [22]. A smaller leakage of thermal flux indicates

better sealing effectiveness of the air curtain. Therefore, the smoke control efficiency can be expressed using the following equations:

$$\eta = 1 - \frac{\Delta E_{Vj}}{\Delta E_{Vk}} \quad (1)$$

$$\Delta E_{Vj} = \frac{1}{Z} \int (q_{Vj}(Z) - q_{Vj=0}(Z)) dz \quad (2)$$

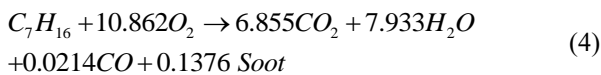
$$\Delta E_{Vk} = \frac{1}{Z} \int (q_{Vk}(Z) - q_{Vk=0}(Z)) dz \quad (3)$$

where,  $\eta$  represents the smoke control efficiency of the air curtain,  $\Delta E_{Vj}$  is the average thermal flux density (kW/m<sup>2</sup>) in the downstream area 5 m below the air curtain,  $\Delta E_{Vk}$  denotes the average thermal flux density (kW/m<sup>2</sup>) in the upstream area 5 m from the air curtain,  $q_{Vj=0}$  and  $q_{Vk=0}$  signify the thermal flux density values (kW/m<sup>2</sup>) under conditions without an air curtain, and  $Z$  represents the effective height (m).

### 2.3 Smoke extraction efficiency of shafts

The efficiency of smoke extraction through shafts was defined using the mass flow rate of CO at the shaft outlets as the standard. The smoke extraction efficiency of the shaft is expressed as the percentage of the total CO emitted per unit time to the total CO produced per unit time. This metric serves as the most direct indicator of smoke extraction effectiveness during a fire, calculated as follows: Smoke extraction efficiency of the shaft outlets = total CO mass flow through all outlets / total CO generated by the fire source per unit time [23].

According to the reaction equation for the incomplete combustion of heptane as follows:



Given that the calorific value of heptane is 45,534.34 kJ/kg, it can be calculated that, for a fire source with a burning power of 10 MW, the CO generated per unit time is 1.3158 g/s. The total mass flow rate of CO discharged from each shaft outlet can then be computed from the onset of the fire, allowing for the determination of the smoke extraction efficiency of the shaft.

### 2.4 Grid division

The size of the grid parameters in FDS fire simulations determines the accuracy of the simulation results. Therefore, appropriate grid parameters must be selected to obtain precise outcomes. Referring to the experimental results of McGrattan et al. [24], the  $D^*/\delta x$  criterion is widely used to estimate the accuracy of grids during large eddy simulations, where  $\delta$  represents the grid size. The characteristic diameter of the fire source,  $D^*/\delta x$ , is generally valued between 4 and 16, expressed as follows:

$$D^* = \left( \frac{Q}{\rho_0 c_p T_0 g^{1/2}} \right)^{2/5} \quad (5)$$

where,  $Q$  is the heat release rate of the fire source (kW);  $\rho_0$  is the air density (kg/m<sup>3</sup>), taken as 1.205 kg/m<sup>3</sup>;  $c_p$  is the specific heat capacity of air (kJ/(kg·K)), taken as 1.003 kJ/(kg·K);  $T_0$  is the ambient temperature (K), taken as 293 K (20°C); and  $g$  is the acceleration due to gravity (m/s<sup>2</sup>), taken as 9.81 m/s<sup>2</sup>.

To establish suitable grid sizes, the case of a fire source with a power of 10 MW was considered. The calculated range for grid size,  $\delta$ , was found to be between 0.15 and 0.62. Given the operational performance and run time of the computer, a grid size of 0.25 × 0.25 × 0.25 was adopted within a 5 m range on both sides of the air curtain, while a grid size of 0.5 × 0.5 × 0.5 was selected for the remaining areas. The simulation duration was set to 360 s.

## 3. IMPACT OF AIR CURTAIN AND SHAFT SPACING ON SHAFT SMOKE EXTRACTION EFFICIENCY

### 3.1 Working condition settings

To investigate the effect of air curtain spacing on the smoke extraction efficiency of shafts, a tunnel model with a fire source power of 10 MW was selected. The air curtain spacing was set symmetrically on both sides of the fire source at 80 m, 90 m, 95 m, 100 m, 105 m, 110 m, 115 m, and 120 m, with an air curtain outlet width of 0.5 m, a jet velocity of 10 m/s, and a jet angle of 20° [25]. The shaft spacing was maintained at 60 m, with a no-shaft smoke extraction condition set as the control group. Thermal flux density monitoring surfaces were established 5 m in front of and behind the air curtain, and CO mass flow measurement points were evenly distributed at the inlet and outlet of the shafts. The simulation conditions are summarized in Table 1.

**Table 1.** Simulated working condition settings

Working Condition Number	Air Curtain Spacing (m)	Shaft Spacing (m)
1	80	No shaft
2	80	60
3	90	60
4	95	60
5	100	60
6	105	60
7	110	60
8	115	60
9	120	60

### 3.2 Result analysis

During the early stages of fire development, the generated smoke rises and impacts the ceiling, subsequently moving in a unidirectional manner towards both ends. As the smoke diffuses, it gradually descends. Within the time frame for personnel self-evacuation, the stable airflow created by the air curtain can confine the smoke to the smoke control area. While providing a more stable escape environment for individuals, the smoke extraction through shafts can also slow down the descent rate of the high-temperature smoke layer, thereby reducing the temperature of both the tunnel ceiling and the escape area for personnel. Based on previous research findings, CO was utilized as a quantitative indicator for the smoke extraction efficiency of shafts. Through FDS simulations, the results of smoke extraction efficiency from shafts, smoke control efficiency by air curtains, and tunnel

temperature distribution after a simulation time of 360 s are presented in Table 2 and Figure 2.

**Table 2.** Efficiency of smoke extraction from shafts and smoke control by air curtains

Working Condition Number	Air Curtain and Shaft Spacing (m)	Smoke Extraction Efficiency from the Shaft (%)	Smoke Control Efficiency by the Air Curtain (%)
1	80	—	46.25
2	80	42.28	86.64
3	90	39.44	89.40
4	95	38.22	89.99
5	100	36.93	90.48
6	105	36.63	90.6
7	110	36.05	90.91
8	115	35.48	90.33
9	120	34.62	90.90
Range of smoke extraction/control efficiency		34.62~42.28	86.64~90.91

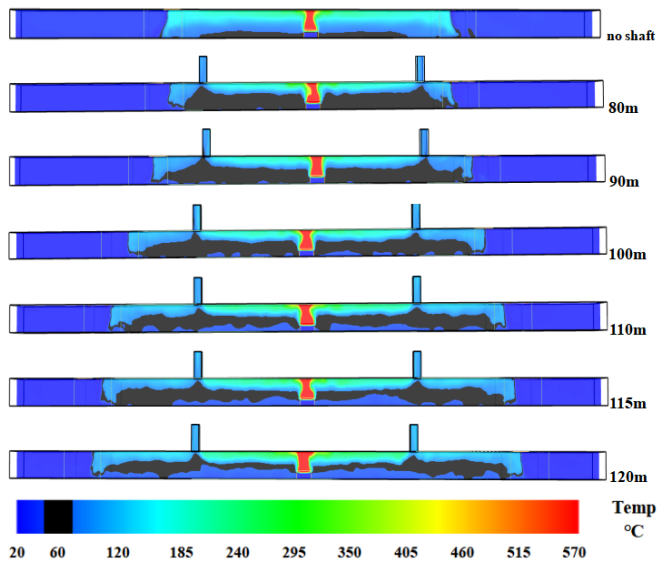


**Figure 2.** Temperature distribution in the tunnel at different air curtain and shaft spacings

It can be observed from Table 2 that when the shaft spacing remains constant, the distance between the shaft and air curtain increases from 10 m to 30 m, resulting in the air curtain's smoke control efficiency stabilizing within the range of 86.64% to 90.91%. However, this smoke control effect diminishes as the distance of the air curtain from the fire source decreases. In comparison to the no-shaft condition, the efficiency of the air curtain increases by 96.5%. The shaft smoke extraction efficiency ranges from 34.62% to 42.28%, with efficiency increasing as the spacing decreases. This indicates that the spacing between the air curtain and shaft significantly influences the smoke extraction efficiency of shafts.

As shown in Table 2, the increase in shaft smoke extraction efficiency with the reduction of air curtain-shaft spacing can be attributed to the significant smoke and heat barrier effect of the air curtain, which achieves up to 90% efficiency. The substantial airflow generated by the air curtain causes high-temperature smoke accumulated in front of it to flow back towards the fire source, resulting in a large volume of high-temperature smoke collecting in the upper layer of the tunnel's smoke control area. As illustrated in the temperature distribution cloud map in the tunnel at different spacings in Figure 2, the overall temperature in the smoke control area shows an upward trend with decreasing air curtain-shaft spacing. According to the ideal gas law  $PV=nRT$ , the pressure

$P$  is directly proportional to the gas temperature  $T$ . Consequently, higher temperatures in the smoke control area lead to increased pressure, resulting in a larger pressure differential between inside and outside the tunnel, thereby enhancing the chimney effect and increasing smoke extraction efficiency of shafts.

Conversely, the temperature distribution depicted in Figure 2 indicates that the overall temperature in the personnel activity zones of both the smoke control and evacuation areas remains below 60°C, meeting evacuation requirements. Additionally, as the spacing between the two air curtains decreases, the overall temperature in the smoke control area rises. The temperature around the shaft exhibits an  $M$ -shaped distribution, with the temperature in the outer evacuation area being significantly lower than that in the smoke control area. In comparison to the no-shaft smoke extraction condition, a substantial reduction in tunnel temperature is observed.

Based on the aforementioned analyses of air curtain smoke control efficiency, shaft smoke extraction efficiency, and minimization of evacuation time, an air curtain spacing of 80 m and a shaft spacing of 60 m were selected for subsequent studies.

#### 4. ANALYSIS OF THE AIR CURTAIN-SHAFT COMBINED SMOKE EXTRACTION EFFECT

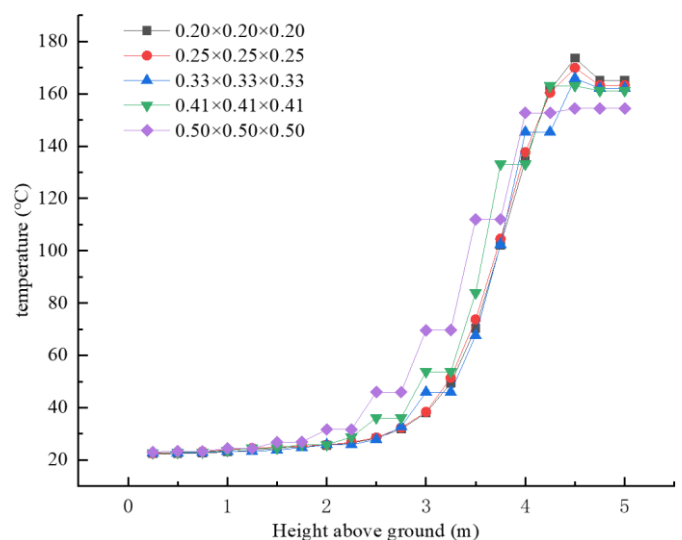


**Figure 3.** Temperature distribution at various heights, measured 30 m from the fire source, under different grid sizes with a heat release rate of 12 MW

#### 4.1 Experimental design and simulation conditions

The jet velocity and angle are identified as the two most critical factors influencing the smoke control effectiveness of air curtains. To investigate the combined smoke extraction effects of air curtains and shafts under realistic tunnel fire conditions, a fire source with a power output of 12 kW was selected for the simulation experiment. The recommended range for the grid size  $\delta$  was calculated to be between 0.16 and 0.64. Figure 3 illustrates the temperature variation at different heights, 30 meters from the fire source, when the fire power was set at 12 MW. When the grid sizes are 0.33, 0.41, and 0.5, the temperature curves do not exhibit smooth transitions, indicating that the grid sizes are too large for precise temperature measurement at varying heights. Conversely, when grid sizes of 0.20 and 0.25 are used, the temperature measurement points connect smoothly, with minimal temperature differences between them, suggesting that these grid sizes offer higher simulation accuracy. To meet measurement accuracy requirements and optimize

computational performance, a grid size of  $0.25 \times 0.25 \times 0.25$  was selected within a 5-meter range on either side of the air curtain and within the shaft, while a grid size of  $0.5 \times 0.5 \times 0.5$  was chosen for the remaining tunnel area.

For the air curtain conditions, a jet width of 0.3 m was selected, with jet angles varying from  $0^\circ$  to  $30^\circ$ , and jet velocities of 6 m/s, 8 m/s, and 10 m/s were employed. Temperature measurement points were placed every 1 m at a height of 0.1 m below the tunnel ceiling. Additionally, at a height of 1.8 m within the tunnel, temperature, visibility, and CO measurement points were arranged every 1 m. At the centre of the shaft, temperature and CO concentration measurement points were positioned vertically every 1 m along the shaft's length. To facilitate a more intuitive observation of the simulation results, a steady-state fire scenario was simulated for a duration of 240 s, while the remaining working conditions were consistent with those described previously. The designed working conditions are summarized in Table 3.

**Table 3.** Simulated working condition settings

Working Condition Number	Air Curtain Spacing (m)	Shaft Spacing (m)	Fire Source Power (kW)	Deflection Angle ( $^\circ$ )	Jet velocity (m/s)
1	—	60	12	—	—
2-5	80	60	12	0/10/20/30	6
6-9	80	60	12	0/10/20/30	8
10-13	80	60	12	0/10/20/30	10

**Table 4.** Smoke extraction/control efficiency under different working conditions

Working Condition Number	Deflection Angle ( $^\circ$ )	Jet Velocity (m/s)	Smoke Extraction Efficiency (%)	Smoke Control Efficiency (%)
1	—	—	30.42	—
2	0	6	66.57	85.81
3	10	6	71.35	92.64
4	20	6	72.59	94.36
5	30	6	73.14	94.61
6	0	8	70.72	91.74
7	10	8	71.79	93.62
8	20	8	72.07	93.47
9	30	8	71.91	92.27
10	0	10	72.58	93.18
11	10	10	71.66	93.41
12	20	10	71.17	93.23
13	30	10	69.47	89.45

#### 4.2 Simulation results and analysis

Through the calculation and organization of simulation results, the smoke extraction efficiency of the shaft and the smoke control efficiency of the air curtain under various conditions are presented in Table 4. The results indicate that the smoke control efficiency of the air curtain remains consistently above 85%, effectively blocking most of the smoke and heat. When the air curtain jet angle is set at  $0^\circ$ , an increase in jet velocity from 6 m/s to 10 m/s results in a corresponding rise in smoke control efficiency. At a jet velocity of 6 m/s, the smoke control efficiency increases with the jet speed, peaking at a jet angle of  $30^\circ$ . At 8 m/s, the efficiency first increases and then decreases with rising jet angles, reaching its maximum at  $10^\circ$ . Conversely, at 10 m/s, the smoke control efficiency begins to decline as the jet angle increases, indicating that the influence of the jet angle on efficiency diminishes with higher air curtain speeds.

Additionally, during the observation of smoke propagation under simulated conditions, it was noted that when smoke begins to leak from the control area, the leak position of the air curtain descends longitudinally as the jet velocity increases. With an increase in jet angle, high-temperature smoke from the low-speed air curtain rises quickly below the ceiling, while smoke from the high-speed air curtain leaks beneath it, mixing with cooler smoke below. This results in a decrease in both smoke temperature and momentum, with a small portion of the leaked smoke temporarily accumulating in the tunnel evacuation area, leading to a reduction in smoke control efficiency. Compared to scenarios without an air curtain, the time for smoke to diffuse into the evacuation area is effectively extended, and the smoke extraction efficiency of the shaft is also greatly improved.

The results indicate that the mass flow rate of air evacuated from the shaft and the smoke extraction efficiency increase with the rise in air curtain velocity, with an overall efficiency

stabilizing above 65%. Compared to the condition without an air curtain, the evacuation efficiency has increased by 140%. This enhancement is attributed to the air curtain, which confines most of the smoke within the smoke control zone, leading to increased smoke concentration and overall temperature, thereby intensifying the chimney effect in the shaft. Additionally, the presence of the air curtain disrupts the layering of smoke near the shaft, allowing more smoke to be expelled from the tunnel. Moreover, it is observed that when the jet velocity of the air curtain is 6 m/s, the shaft's evacuation efficiency increases with the rise in jet angle. At a jet velocity of 8 m/s, the peak evacuation efficiency occurs at a jet angle of 20°, followed by a slight decline. However, when the jet velocity is increased to 10 m/s, the extraction efficiency decreases as the jet angle increases. The correlation between the air curtain's smoke control efficiency and the shaft's smoke extraction efficiency is consistent, suggesting that the extraction efficiency is closely related to the sealing effect of the air curtain on the smoke.

Previous research has established that the smoke extraction efficiency of shafts is related to the longitudinal wind speed and the separation of smoke layers [26]. Further simulations indicate that, for a fire source power of 12 kW, the critical wind speed falls between 2.5 m/s and 3 m/s. When the air curtain jet velocity is set at 6 m/s, the longitudinal velocity components for jet angles ranging from 0° to 30° remain less than or equal to 3 m/s. At a jet velocity of 8 m/s, the longitudinal velocity components for jet angles from 0° to 20° also remain below 3 m/s. As the jet angle increases, the longitudinal wind component likewise increases, resulting in a rise in smoke concentration at the shaft outlet compared to the condition without a longitudinal wind component. This leads to an increased pressure differential between the interior and exterior of the shaft, thereby enhancing the chimney effect and improving the extraction efficiency. Conversely, when the air curtain jet velocity is increased to 10 m/s, the excessive longitudinal velocity results in a greater mixing of smoke and air, leading to a decrease in smoke concentration beneath the shaft outlet. Fresh air ejected by the air curtain is drawn into the shaft, exacerbating the phenomenon of entrainment. Consequently, the shaft's smoke extraction efficiency diminishes as the jet angle increases.

### 4.3 Distribution of temperature, visibility, and CO concentration in the tunnel under different working conditions

#### 4.3.1 Temperature variation below the ceiling (average temperature at various locations over 240 s)

Figure 4 illustrates the temperature distribution beneath the ceiling at different jet velocities. Given that the selected air curtain jet velocities are not significantly different, the variations in tunnel temperature under the influence of air curtains are minimal, yet a noticeable trend is observed. The tunnel can be divided into two sections based on temperature distribution: one section falls within the shaft spacing and the other extends beyond it. It is evident from the figure that in the region outside the shaft spacing, the temperature beneath the ceiling decreases significantly with increasing jet velocity. The tunnel temperature under low-velocity air curtains is generally higher than that under high-velocity ones. Additionally, the temperature of smoke near the air curtain and the shaft drops by approximately 90°C and 70°C, respectively, indicating that the injection of cool air and the extraction of

smoke through the shaft can effectively reduce the tunnel temperature. The temperature near the shaft stabilizes around 100°C, while the temperature close to the air curtain remains around 22°C. In the section of the tunnel within the shaft spacing, as the jet velocity increases, the sealing effect of the air curtain improves, resulting in a higher tunnel temperature under high-velocity air curtains compared to that under low-velocity ones.

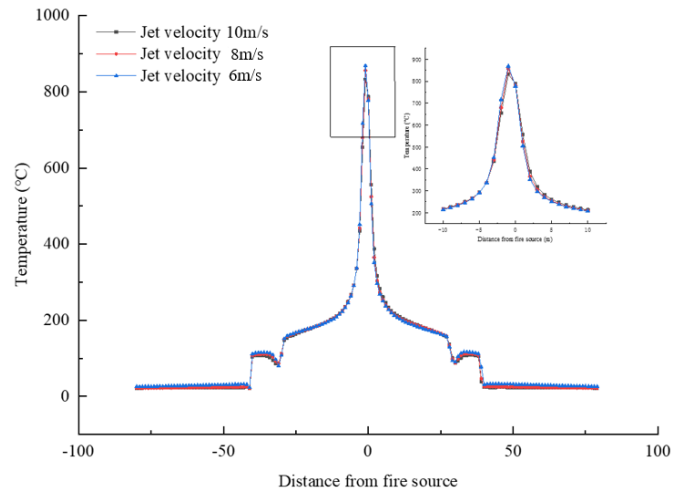
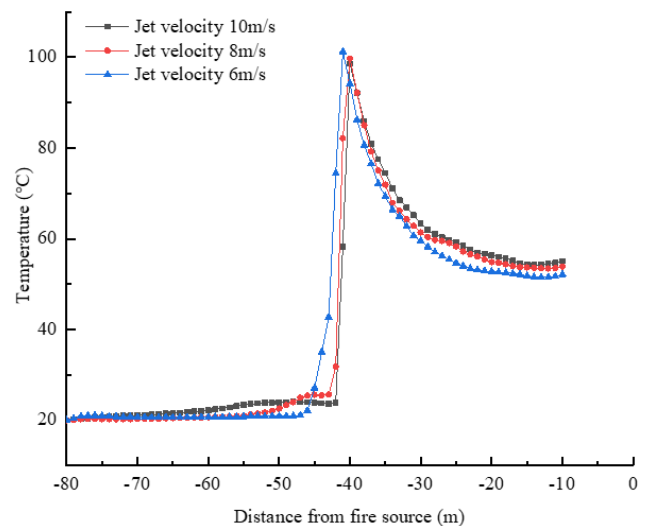
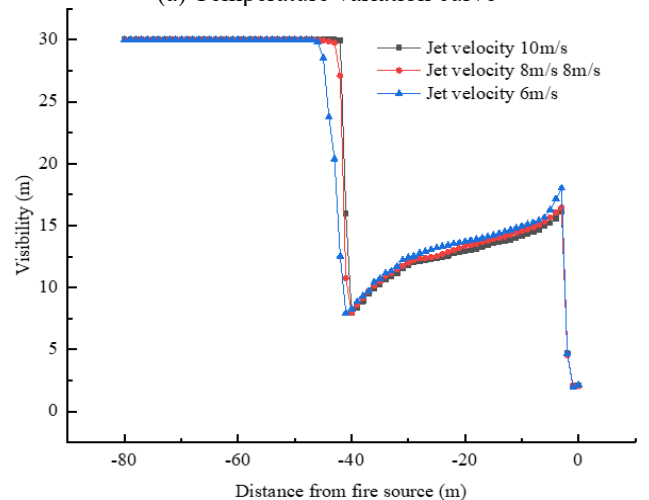


Figure 4. Temperature distribution below the ceiling at different jet velocities

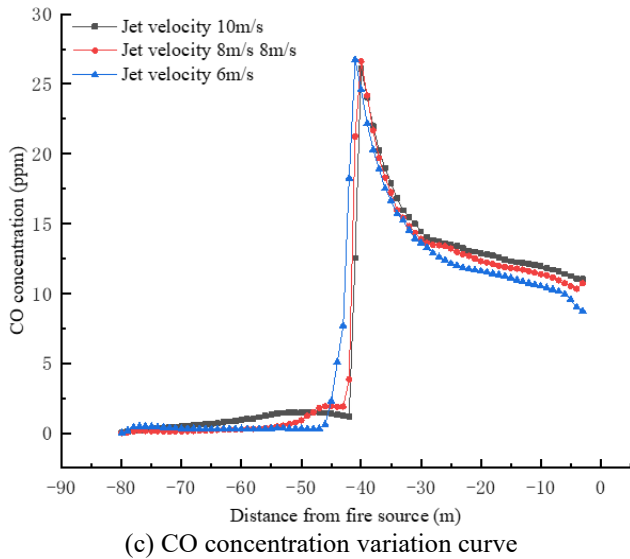


(a) Temperature variation curve



(b) Visibility variation curve





(c) CO concentration variation curve

**Figure 5.** Variation curves of smoke temperature, visibility and CO concentration at eye level under different jet velocities

#### 4.3.2 Distribution patterns of temperature, visibility, and CO concentration at eye level in the tunnel

Figures 5(a)-(c) depict the distribution of temperature, visibility, and CO concentration, respectively, at a height of 1.8 m above the ground under different jet velocities. Due to the symmetrical structure of the simulated working conditions, the left side of the tunnel was selected for analysis. To enhance data accuracy, average values from different measurement points over 240 s were utilized for graphical representation.

As observed in Figure 5(a), with an increase in jet velocity, the smoke control efficiency of the air curtain is enhanced, resulting in higher overall temperatures at eye level for the high-velocity air curtain compared to the low-velocity one. It is also evident that the smoke extraction from the shaft has minimal impact on the lower temperatures within the tunnel. In the area designated for personnel movement, the temperature on the left side of the air curtain remains stable between 20°C and 30°C, while the temperature in the smoke control zone on the right side remains below 100°C. A temperature rise of approximately 20°C occurs on both sides of the air curtain, attributed to the attenuation of jet momentum during the airflow process, coupled with the impact of hot smoke, which causes deflection of the air curtain's range. The planar jet of the air curtain obstructs the lateral flow of smoke, causing accumulation beneath the curtain, which results in temperatures in proximity to the air curtain being significantly higher than those at either end. It is noteworthy that temperatures near the low-velocity air curtain exceed those near the high-velocity one, as the cold air injected by the high-velocity air curtain is greater, allowing for more effective cooling when mixed with the high-temperature smoke.

Figure 5(b) illustrates the visibility variation at eye level under different jet velocities. It is apparent that, except for areas near the air curtain's heat source, visibility within the tunnel exceeds 10 m, with visibility in the evacuation area on the left side of the air curtain stabilizing around 27 m. Furthermore, as the jet velocity of the air curtain increases, its sealing effectiveness improves, leading to a decrease in visibility within the smoke control zone. Conversely, the visibility in the evacuation area shows an opposite trend.

Figure 5(c) illustrates the variation of CO concentration at

eye level under different jet velocities. Based on standards regarding the harmful effects of CO on human health, a threshold of 50 ppm was selected as the safety limit for evacuating personnel. The data indicate that the CO concentration within the tunnel remains consistently around 30 ppm, significantly below the evacuation threshold, thus meeting the conditions for safe escape. As the jet velocity increases, peak CO concentrations near the heat source reach values of 272.71 ppm, 268.51 ppm, and 264.4 ppm, respectively. In contrast, CO concentrations in the vicinity of the air curtain decrease as the jet velocity increases, which aligns with the temperature distribution pattern.

CO is a byproduct of incomplete combustion from the heat source; thus, the smoke concentration can be represented by CO levels. It is evident that the CO concentration in the tunnel correlates with the temperature distribution pattern but inversely relates to visibility. This discrepancy arises because the tunnel temperature is primarily influenced by the smoke, with the high-temperature smoke generated during combustion diffusing within the tunnel under pressure, thereby elevating the overall temperature. When smoke concentration becomes excessively high, the presence of solid and liquid particles within the smoke leads to obscuration, as these particles can scatter and absorb visible light, resulting in reduced visibility within the tunnel.

## 5. CONCLUSION

As a traditional smoke extraction method, shafts have certain limitations in creating a safe escape environment for personnel. This study combines shafts with air curtains based on theoretical analysis and establishes various tunnel fire working conditions using software. The research investigates the impact of air curtain parameters on shaft smoke extraction efficiency and examines the distribution patterns of temperature, visibility, and CO concentration within a combined smoke extraction system. The main conclusions are as follows:

- Under constant shaft spacing, a comparative study of various air curtain-shaft spacing working conditions reveals that as the spacing decreases, the air curtain's smoke control efficiency declines, while the shaft's smoke extraction efficiency increases. Compared to working conditions without shafts, the air curtain's smoke control effectiveness improves by 96.5%, validating the feasibility of the combined air curtain-shaft smoke extraction model.

- By comparing the smoke extraction efficiency from shafts and the smoke control efficiency by air curtains under a heat source power of 12 kW, it is evident that the air curtain's smoke control efficiency increases with the jet velocity. At a jet velocity of 6 m/s, both efficiencies increase with the jet angle, with an optimal jet angle of 30°. At a jet velocity of 8 m/s, the smoke control and extraction efficiencies exhibit an initial increase followed by a decrease as the jet angle increases, peaking at 20°. When the air curtain jet velocity is 10 m/s, both efficiencies decrease with increasing jet angle. Compared to conditions without an air curtain, shaft extraction efficiency increases by 140%. Overall, the trends in the smoke extraction efficiency of shafts are consistent with those observed for the smoke control efficiency of air curtains.

- Based on a comparison of temperature distribution beneath the tunnel ceiling at different jet velocities, it can be observed that in the tunnel sections outside the shaft spacing, the

temperature beneath the ceiling significantly decreases as the jet velocity increases. A marked drop in temperature occurs at both the shaft and air curtain locations. Conversely, within the tunnel space defined by the shaft spacing, the temperature under high-velocity air curtains is higher than that under low-velocity ones, although the peak temperature above the heat source decreases with increasing wind speed.

•Within the tunnel space at eye level, the temperature increases with the increase in air curtain jet velocity, and the temperature near the air curtain is considerably higher due to the impact of hot smoke. Additionally, it can be observed that the visibility in the smoke control area decreases as the air curtain jet velocity increases, while the visibility in the evacuation area exhibits an opposite trend. The CO concentration within the tunnel increases with the rise in air curtain jet velocity. However, the CO concentration near the air curtain decreases with increasing jet velocity, consistent with the observed temperature distribution patterns.

## REFERENCE

- [1] Xu, T., Tang, F., Xu, X., He, Q. (2023). Impacts of ambient pressure on the stability of smoke layers and maximum smoke temperature under ceiling in ventilated tunnels. *Indoor and Built Environment*, 32(1): 85-97. <https://doi.org/10.1177/1420326X211013080>
- [2] Ma, D., Duan, H., Zhang, J. (2022). Solid grain migration on hydraulic properties of fault rocks in underground mining tunnel: Radial seepage experiments and verification of permeability prediction. *Tunnelling and Underground Space Technology*, 126: 104525. <https://doi.org/10.1016/j.tust.2022.104525>
- [3] Hu, L.H., Zhou, J.W., Huo, R., Peng, W., Wang, H.B. (2008). Confinement of fire-induced smoke and carbon monoxide transportation by air curtain in channels. *Journal of hazardous materials*, 156(1-3): 327-334. <https://doi.org/10.1016/j.jhazmat.2007.12.041>
- [4] Guo, Q., Zhu, H., Zhang, Y., Shen, Y., Zhang, Y., Yan, Z. (2020). Smoke flow in full-scale urban road tunnel fires with large cross-sectional vertical shafts. *Tunnelling and Underground Space Technology*, 104: 103536. <https://doi.org/10.1016/j.tust.2020.103536>
- [5] Wang, M., Guo, X., Yu, L., Zhang, Y., Tian, Y. (2021). Experimental and numerical studies on the smoke extraction strategies by longitudinal ventilation with shafts during tunnel fire. *Tunnelling and Underground Space Technology*, 116: 104030. <https://doi.org/10.1016/j.tust.2021.104030>
- [6] Zhu, B., Cong, H., Yu, B., Shao, Z., Ye, L., Bi, Y., Zeng, Y. (2024). Experimental study on the performance of synergistic ventilation system combining shaft with mechanical ventilation in extra-long road tunnels. *Tunnelling and Underground Space Technology*, 147: 105706. <https://doi.org/10.1016/j.tust.2024.105706>
- [7] Zhang, S., He, K., Yao, Y., Peng, M., Yang, H., Wang, J., Cheng, X. (2018). Investigation on the critical shaft height of plug-holing in the natural ventilated tunnel fire. *International Journal of Thermal Sciences*, 132: 517-533. <https://doi.org/10.1016/j.ijthermalsci.2018.06.018>
- [8] Zhao, S., Xu, L., Obadi, I., Wang, F., Liu, F., Weng, M. (2021). Plug-holing height and complete plug-holing phenomenon in naturally ventilated tunnel fires with vertical shaft. *Tunnelling and Underground Space Technology*, 107, 103631. <https://doi.org/10.1016/j.tust.2020.103631>
- [9] Kashef, A., Yuan, Z., Lei, B. (2013). Ceiling temperature distribution and smoke diffusion in tunnel fires with natural ventilation. *Fire Safety Journal*, 62: 249-255. <https://doi.org/10.1016/j.firesaf.2013.09.019>
- [10] Takeuchi, S., Aoki, T., Tanaka, F., Moinuddin, K.A. (2017). Modeling for predicting the temperature distribution of smoke during a fire in an underground road tunnel with vertical shafts. *Fire Safety Journal*, 91: 312-319. <https://doi.org/10.1016/j.firesaf.2017.03.063>
- [11] Tanaka, F., Harada, N., Yamaoka, S., Moinuddin, K.A. (2024). Fire control and self-extinguishment by blocking smoke flow with water spray in a tunnel fire. *Fire Safety Journal*, 142: 103999. <https://doi.org/10.1016/j.firesaf.2023.103999>
- [12] Mohammadi, P.K.M., Khalilpour, S.H., Parsa, H., Sareh, P. (2022). Protective water curtains as wave attenuators for blast-resistant tunnels. *Scientific Reports*, 12(1): 20463. <https://doi.org/10.1038/s41598-022-24943-7>
- [13] Elicer-Cortés, J.C., Molina, N., Severino, G., Fuentes, A., Rojas, P. (2020). Turbulent transport mechanisms on the heat confinement in tunnels by using low-velocity air curtains. *Applied Thermal Engineering*, 181: 115852. <https://doi.org/10.1016/j.applthermaleng.2020.115852>
- [14] Chen, Z., Liu, Z., Huang, L., Niu, G., Yan, J., Wang, J. (2023). Research on the effect of ceiling centralized smoke exhaust system with air curtains on heat confinement and plug-holing phenomenon in tunnel fires. *Process Safety and Environmental Protection*, 169: 646-659. <https://doi.org/10.1016/j.psep.2022.11.054>
- [15] Severino, G., Elicer-Cortés, J.C., Fuentes, A. (2013). Characterization of a diffusion flame inside a scale tunnel using double stream-twin jets air curtains. *Fire Safety Journal*, 62: 264-271. <https://doi.org/10.1016/j.firesaf.2013.09.014>
- [16] Ji, J., Lu, W., Li, F., Cui, X. (2022). Experimental and numerical simulation on smoke control effect and key parameters of Push-pull air curtain in tunnel fire. *Tunnelling and Underground Space Technology*, 121: 104323. <https://doi.org/10.1016/j.tust.2021.104323>
- [17] Luo, N., Li, A., Gao, R., Tian, Z., Zhang, W., Mei, S., Feng, L., Ma, P. (2013). An experiment and simulation of smoke confinement and exhaust efficiency utilizing a modified Opposite Double-Jet Air Curtain. *Safety Science*, 55: 17-25. <https://doi.org/10.1016/j.ssci.2012.12.002>
- [18] Shoshe, M.A.M.S., Rahman, M.A. (2022). Air curtain in informal shopping malls: Optimization of the air curtain operating parameters for heat and smoke confinement. *Energy and Buildings*, 276: 112531. <https://doi.org/10.1016/j.enbuild.2022.112531>
- [19] Viegas, J.C., Cruz, H. (2019). Air curtains combined with smoke exhaust for smoke control in case of fire: Full-size experiments. *Fire Technology*, 55: 211-232. <https://doi.org/10.1007/s10694-018-0786-z>
- [20] Yu, L. X., Liu, F., Beji, T., Weng, M.C., Merci, B. (2018). Experimental study of the effectiveness of air curtains of variable width and injection angle to block fire-induced smoke in a tunnel configuration. *International Journal of Thermal Sciences*, 134: 13-26. <https://doi.org/10.1016/j.ijthermalsci.2018.07.044>
- [21] Brzezinska, D., Ollesz, R., Bryant, P. (2020). Design car fire size based on fire statistics and experimental data.



- Fire and Materials, 44(8): 1099-1107. <https://doi.org/10.1002/fam.2913>
- [22] Gao, D., Li, T., Mei, X., Chen, Z., You, S., Wang, Z., Wang, K., Lin, P. (2020). Effectiveness of smoke confinement of air curtain in tunnel fire. *Fire technology*, 56: 2283-2314. <https://doi.org/10.1007/s10694-020-00977-z>
- [23] Gao, Z., Zhao, P., Wu, Z., Cai, J., Li, L. (2024). Study on the natural smoke exhaust performance of board-coupled vertical shaft in high-altitude tunnel fires. *Fire*, 7(8): 274. <https://doi.org/10.3390/fire7080274>
- [24] McGrattan, K.B., McDermott, R.J., Weinschenk, C.G., Forney, G.P. (2013). *Fire Dynamics Simulator Users Guide*, Sixth Edition. Special Publication (NIST SP). <https://doi.org/10.6028/NIST.sp.1019>
- [25] Chen, Z., Liu, Z., Li, X., Linqi, H., Niu, G. (2022). Numerical study of the effect of air curtains on smoke blocking and leakage heat flux in tunnel fires. *Case Studies in Thermal Engineering*, 35: 102164. <https://doi.org/10.1016/j.csite.2022.102164>
- [26] Ji, J., Gao, Z.H., Fan, C.G., Zhong, W., Sun, J.H. (2012). A study of the effect of plug-holing and boundary layer separation on natural ventilation with vertical shaft in urban road tunnel fires. *International Journal of Heat and Mass Transfer*, 55(21-22): 6032-6041. <https://doi.org/10.1016/j.ijheatmasstransfer.2012.06.014>